JOURNAL OF THE ROYAL SOCIETY Interface

FirstCite® e-publishing

J. R. Soc. Interface
doi:10.1098/rsif.2011.0148
Published online

Intracellular pH distribution as a cell health indicator in *Saccharomyces cerevisiae*

Thomas Aabo[1,*], Jesper Glückstad[2], Henrik Siegumfeldt[1] and Nils Arneborg[1]

[1]*Department of Food Science, University of Copenhagen, Frederiksberg, Denmark*
[2]*Department of Photonic Engineering, DTU Fotonik, Technical University of Denmark, Kongens Lyngby, Denmark*

Internal pH regulation is vital for many cell functions, including transport mechanisms and metabolic enzyme activity. More specifically, transport mechanisms are to a wide degree governed by internal pH distributions. We introduce the term standard deviation of the intracellular pH (s.d.(pH_{int})) to describe the internal pH distributions. The cellular pH distributional response to external stress such as heat has not previously been determined. In this study, the intracellular pH (pH_i) and the s.d.(pH_{int}) of *Saccharomyces cerevisiae* cells exposed to supralethal temperatures were measured using fluorescence ratio imaging microscopy (FRIM). An exponential decline in pH_i was observed after an initial small decline. For the first time, we report the use of FRIM for determining *in vivo* plasma membrane proton permeability coefficients in yeast. Furthermore, the exponential decay of pH_i and the rupture of the cell plasma membrane, as measured by propidium iodide staining, at 70°C were not simultaneous but were separated by a significant temporal difference. Finally, a nonlinear relationship between the pH_i and s.d.(pH_{int}) was found; i.e. the s.d.(pH_{int}) was significantly more sensitive to supralethal temperatures than pH_i. s.d.(pH_{int}) is therefore proposed as an early health/vitality indicator in *S. cerevisiae* cells exposed to heat stress.

Keywords: heat stress; intracellular pH; permeability; membrane; yeast

1. INTRODUCTION

Numerous methods exist for measuring cell health state and death. However, one of the problems is that cell death is not clearly defined, and different methods will give different answers. Microscopy methods of characterizing viability include among others: membrane integrity detection by DNA intercalating probes, protein expression by GFP (Green Fluorescent Protein), dielectric measurements [1] and intracellular pH (pH_i) measurements [2,3].

In one of the more widely used methods, the probe propidium iodide (PI) is used, which only passes ruptured cell membranes and intercalates into double-stranded DNA, after which it starts to fluoresce. This method is normally referred to as a live/dead staining. However, it is known that cells can be non-culturable before the membrane ruptures and therefore not PI-stained [4,5]. PI and similar acting probes do therefore not always give an accurate representation of the health state of a cell.

Yeast maintain a pH gradient (ΔpH); i.e. pH_i – external pH (pH_{ex}), across the cell membrane [6,7]. The yeast plasma membrane H^+-ATPase is essential for the maintenance of ΔpH, as it will actively pump out H^+ using ATP [8]. The pH_i is of vital importance to the cell and the use of pH_i as an indicator for the general health of a cell is widely used. If the cell has problems generating ATP to drive the H^+-ATPase or the H^+-ATPase is non-functional, the cell will not be able to maintain the ΔpH and the pH_i will drift toward the pH_{ex}. The ability of a cell to maintain the ΔpH has been studied under numerous stressful environmental conditions, e.g. salt stress, heat stress and increased CO_2 pressure [7,9,10].

Several fluorescent probes exist that have absorption and emission spectra that vary depending on the pH of the immediate environment [11]. In this study, we have used the probe 5-(and-6)-carboxyfluorescein diacetate, succinimidyl ester (CFDA-SE), which has several advantages when performing internal staining of cells. The molecule is neutral and is therefore cell permeant. Once inside the cell, intracellular esterases cleave the diacetate groups leaving the molecule (5-(and-6)-carboxyfluorescein, succinimidyl ester; CF-SE) charged and therefore less likely to pass the cell membrane. Furthermore, succinimidyl ester will attach to amine groups in the cells, thereby increasing the period in which the molecule is retained in the cell even if the cell wall or cell membrane is ruptured. Another advantage of using CFDA-SE is that the probe is only fluorescent when the diacete groups have been cleaved off, thereby reducing background noise. The fluorescent active part of the molecule is fluorescein. This

*Author for correspondence (taa@life.ku.dk).

Received 16 March 2011
Accepted 8 April 2011

fluorophore has an absorption spectrum that is dependent on the pH. The fluorophore is exited with two different wavelengths; i.e. 435 and 485 nm, where 435 nm absorption is relatively independent of pH and 485 nm absorption is more pH dependent. The ratio between the intensities at the two different wavelengths therefore has a direct correlation to the pH. Thus, this method has been entitled fluorescence ratio imaging microscopy (FRIM) [2].

Heat stress of yeast has been shown to give an increased plasma membrane proton permeability [12] and a deactivation of the plasma membrane H^+-ATPase [13]. These factors will eventually lead to equilibration of the ΔpH. However, the immediate pH response of yeast to heat stress at supralethal temperatures has to our knowledge only been performed using phosphorus-31 nuclear magnetic resonance (^{31}P NMR) techniques, which have limited temporal resolution [14].

Here, we examine the time dependence at different temperatures of the correlation between pH_i and PI as detection parameters for yeast cell viability. Furthermore, we introduce a new metric for early detection of the 'health state' of a cell, namely, the s.d.(pH_{int}), which is the standard deviation of the intracellular pH distribution in single cells. Finally, we examine the relationship between pH_i and s.d.(pH_{int}) at supralethal temperatures.

2. MATERIAL AND METHODS

2.1. Strain and growth conditions

The yeast strain *Saccharomyces cerevisiae* S288C was used. The growth medium was YPG: yeast extract 3 g l^{-1}, peptone 5 g l^{-1} and glucose 10 g l^{-1}, adjusted to pH 5.6 using 0.1 M HCl. Cells were initially taken from a frozen culture and inoculated into a YPG media. After 24 h the cells were inoculated at 1×10^5 cell ml^{-1} in fresh YPG media and then incubated under aerobic conditions in a shaking water-bath at 25°C at 120 r.p.m. The cells were then harvested in the exponential phase at OD_{600} 0.1.

2.2. Staining and heating procedure

The exponential cells were resuspended in a citrate/phosphate buffer (McIlvaine buffer) pH 5.4 [15]. The cells were then incubated in McIlvaine buffer, pH 7, with 40 µM CFDA-SE (Invitrogen C1157; stock 4 mM in DMSO) for 30 min at 30°C. Preliminary experiments showed that the optimum incubation pH was pH 7 without any observable damage or drop in pH of the cells (data not shown). The cells were then resuspended in McIlavaine buffer pH 5.5, 1 mM glucose and 20 µM PI (Invitrogen P3566, stock concentration 2 mM in H_2O) and loaded into a sample chamber consisting of two 25 × 40 mm coverslips (Menzel-Gläser, no. 1, BB025040A1) separated by a double-sided adhesive tape. The chamber was then sealed with silicone. After the chamber was sealed, the cells were left for 30 min to stabilize their pH_i before placing them on the microscope. The first image was taken at $t = 0$ min. At $t = 1$ min, the heating stage was turned on and at $t = 3$ min, the heating stage had reached its temperature that was maintained for the whole experiment. This was done for all three temperatures investigated (50°C, 60°C and 70°C) and the control temperature (30°C).

2.3. Fluorescence ratio imaging microscopy

A non-standard fluorescence microscope was used to acquire images [16]. The excitation source was a monochromator (polychrome II) from Till photonics. It was controlled using a D/A board that was controlled using a specially written software in LabVIEW. In order to collect the fluorescence signal from both CF-SE and PI, two filter blocks were used. For the CF-SE, a dichroic 505 nm long-pass (Omega optical XF2010) and an emission band-pass filter 515–565 (Zeiss) were used. For the PI, a dichroic 570 nm long-pass (Omega optical XF2015) and an emission long-pass 590 nm filter (XF3016, Omega optical) were used. The excitation wavelength for PI was 535 nm. The objective used was an air objective neofluar 40× N.A. 0.75 from Zeiss. This gave a theoretical resolution of approximately 340 nm. The emission was collected with a QICAM FAST. The exposure times were 1 s at 435 nm and 0.25 s at 485 nm. The binning was set to 2, giving a resolution of 696 × 520 (square pixels). The optical geometry of the set-up gave a projected pixel size at the focal plane of 232 nm.

In order to correlate intensity ratios to pH, it is necessary to create a calibration curve linking the fluorescence intensity ratio to the pH. It is necessary for this to be done *in situ* as the spectral properties as well as the pK_a may be affected by the internal environment of the cell. The cells were spun down and resuspended in 70 per cent ethanol, which will rupture the membrane and equilibrate the pH_i and pH_{ex}. The cells were then divided into the appropriate number of aliquots, resuspended in pH buffers ranging from pH 5 to pH 8, loaded into sample chambers and ratio images were taken of the cells as described above. Figure 1 shows the calibration of *S. cerevisiae* cells at eight different pH values. The data were fitted by a sigmoidal function [17] given by

$$\mathrm{pH} = pK_a \left(\frac{R - R_{\min}}{R_{\max} - R} \right)^{1/S} \quad \text{and} \qquad R = \frac{I_{\lambda 1} - B_{\lambda 1}}{I_{\lambda 2} - B_{\lambda 2}}, \tag{2.1}$$

where pK_a is the acid disassociation constant between the monoanion and dianion of CF-SE. $I_{\lambda 1}$ and $I_{\lambda 2}$ are the intensities collected from excitation with 435 and 485 nm, respectively, and $B_{\lambda 1}$ and $B_{\lambda 2}$ are the background intensities. R is the ratio background-corrected ratio between 435 and 485 nm excitation. $R_{\min}$ and $R_{\max}$ are the limiting ratio values of the high and low pH, respectively. S is the slope of the curve in the linear regime around the pK_a. Fitting the sigmoidal function gives a pK_a of CF-SE of 7.4, which is comparable to other findings [18,19].

The temperature dependence of CF-SE and the buffers were also evaluated. This was done by incubating

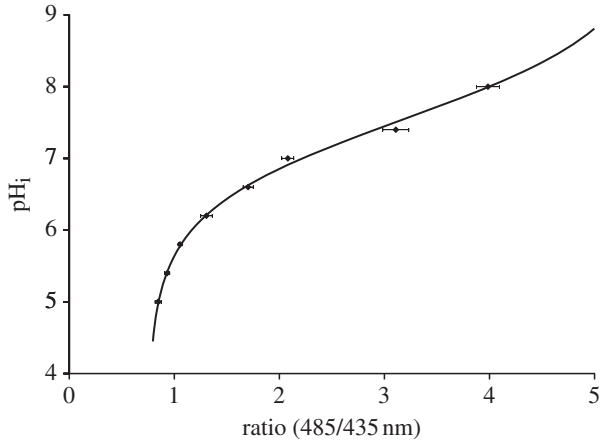

Figure 1. Calibration of CFDA-SE probe. Each data point is an average of 40 cells. The error bars are the standard error mean.

stained cells that had ruptured membranes in buffers with pH values of 5.5 and 7. The pH_i was then measured at 30°C and 70°C. The temperature dependence was considerably smaller than the standard deviation of the calibration curve (data not shown).

2.4. Image analysis

The raw 435 nm image was used to create the mask image. First, background noise was removed by calculating a second-order polynomial that was fitted to nine background points in the image. This was then extrapolated to all pixels in the image, which was then subtracted from the original. In order to define the pixels for the mask of the background-corrected image, we used the thresholding algorithm niblack [20], which gave a mask image that included some noise pixels outside the mask regions. These were removed with the binary functions 'erode' and 'dilate' in that order. The mask image was compared with bright-field images and did not include pixels outside the cells. The mask was then used on both the 435 and 485 nm image to create the ratio image used for calculating pH_i values.

2.5. Heating stage

In the construction of the heating stage, it was essential that the stage reached the set temperature relatively quickly and with no overshoot, as this would alter the measurements drastically. The stage is custom made and has the ability to change the temperature ± 40°C from ambient within 2 min without a temperature overshoot. Once a stable temperature is reached, the chamber is stable within ± 0.2°C. For more details, see Aabo *et al.* [16].

2.6. pH_i decay rate

Several models exist that have been proposed to describe the complex diffusion of ions across a lipid membrane [21,22]. We modelled the pH_i drop; i.e. the pH_i decay rate, using a simple, single exponential function [23–26]. The decay rate constants found in table 1

Table 1. The calculated decay rate constants (k), plasma membrane proton permeability coefficients (P) and goodness of fit (R^2) from exponential decay functions depicted in figure 4.

temperature	k (s^{-1})	R^2	P (cm s^{-1})
50°C	0.036	0.989	3.00×10^{-6}
60°C	0.117	0.997	9.75×10^{-6}
70°C	0.365	0.991	2.96×10^{-5}

were obtained by fitting a single exponential decay function to the data in figure 4 of the form

$$\Delta\mathrm{pH}(t) = \Delta\mathrm{pH}(t_0)\mathrm{e}^{-kt}, \tag{2.2}$$

where $\mathrm{pH}(t_0)$ is the start of the exponential decay at the different temperatures and k is the decay rate constant. As the membrane thickness is much smaller than the cell diameter, the pH_i decay rate constant is linked to the plasma membrane proton permeability coefficient (P) [23] by

$$k = P\frac{S}{V} = \frac{3P}{r}, \tag{2.3}$$

where r is the radius, S is the surface area and V is the volume of the average *S. cerevisiae* S288C cells ($r = 2.5$ μm).

The regulation of the pH_i does not only depend on the activity of the H^+-ATPase and the permeability of the membrane to protons. The proton-motive force, which is the driving force for proton diffusion, is dependent on both the membrane potential and the proton gradient. The diffusion of protons to equilibrate pH will create an increase in membrane potential, if counter ions are not moved out through the membrane at the same rate as the protons. If the permeability of dominant ions (K^+, Mn^{2+}, Mg^{2+}, Cl^-) is much lower than proton permeability, the rate-limiting factor in the pH drop will then be the permeability of these counter ions [21]. As we calculate the permeability directly from the decay rate constant, we do not account for this possible effect in our model. Furthermore, the buffering capacity of the cell should be taken into account. The buffering capacity is the ability of a cell to maintain a pH value by buffering the protons. This effect is normally accredited to the negative charges on the outside of proteins [27]. Given these complications, we do not intend to determine specific H^+ permeabilities, as this would entail the inclusion of a complex model and a specific constant for buffering capacities, ion permeabilities, membrane capacitance and temperature dependence, which is out of the scope of this article. Furthermore, many of these parameters are not known for *S. cerevisiae*.

2.7. Standard deviation of the intracellular pH

The standard deviation of the pH within a cell; i.e. the $\mathrm{s.d.}(\mathrm{pH_{int}})$, is defined as

$$\mathrm{s.d.}(\mathrm{pH_{int}}) = \sqrt{\frac{\sum_{i=1}^{n}(x_i - m)^2}{n-1}}, \tag{2.4}$$

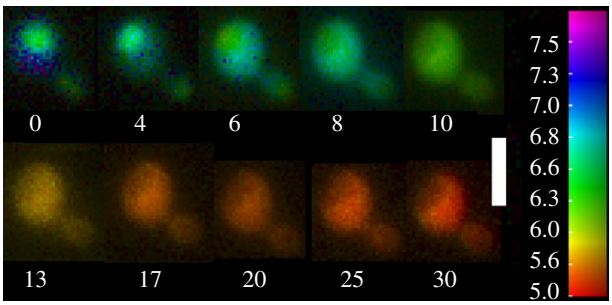

Figure 2. Time line of a single *S. cerevisiae* S288C cell exposed to 60°C. The number below the cell is the time in minutes after $t = 0$. The intensity represents the concentration of probe and the colour represents the pH_i. The white size bar is 5 μm.

where x is the ratio value of the single pixel, m is the mean ratio value of the whole cell and n is the number of pixels within a single cell. This was used as a metric to describe the internal distributions of the pH values within a cell. The value of s.d.(pH_{int}) will be high, if large variations in pH exist within a cell owing to organelles with a pH value different from the cytosolic pH. This is the normal scenario for non-stressed cells. If the s.d.(pH_{int}) is low, it indicates that pH variations between organelles and cytosol are either small or completely removed.

3. RESULTS

In figure 2, the pH_i of a single *S. cerevisiae* S288C cell is followed over 30 min exposed to 60°C. Figure 2 is an example of the pH distribution within a cell as observed with our set-up. Owing to large temperature variation of the heating stage constraining us to use air objectives, the numerical aperture was only 0.75. This resulted in a resolution that was not high enough to measure specific cytosolic and vacuolar pH values of all the cells. At $t = 0$, the cell had two pH regions. The vacuole (green colour) had a pH of around 6.8, and the cytosol (dark blue colour) had a pH of around 7.2. Within 10 min, the cell cytosol pH changed from 7.2 to 6.7; however, the vacuolar pH did not change with the same rate as the cytosol but remained close to 6.8 for the first 8 min. After 10 min, a dark spot appeared where the vacuole was placed (validated by bright-field images, data not shown), and the pH was similar to that of the cytosol. From 11 to 30 min, the pH_i distribution was very homogeneous as the pH_i fell from 6.7 to 5.6. The dark spot was present in all images from $t = 10$ min, as the fluorescence intensity decreased at both 435 (close to the isosbestic wavelength) and 485 nm, which indicated the absence of the probe inside the vacuole. These results suggest that the vacuolar membrane has become more permeable to the probe as a result of heating. It should be stressed, however, that from our results it is not possible to conclude whether the vacuolar membrane has ruptured, or whether the absence of the probe within the vacuole is just a consequence of the increased diffusion of the probe coupled with increased permeability.

In figure 3, four histograms are plotted of the pH_i distributions within the same cell as shown in figure 2 at different times. Figure 3 is intended as an example of the pH_i distribution development of a single cell and serves to illustrate the level of pH resolution within a single cell of our set-up, using objectives with a relatively low numerical aperture of 0.75. The histograms were first calculated as ratios and then transformed into pH values by using equation (2.1). The pH_i distribution within the cell started off with a large standard variation s.d.(pH_{int}) = 0.19. The large s.d.(pH_{int}) value was owing to the cytosolic and vacuolar pH differences, an example of which is shown in figure 2. No clear peaks in the histogram representing vacuolar or cytosolic pH were seen at $t = 0$. However, the pH_i distribution was not Gaussian. At $t = 5$ min, the cells pH_i had shifted slightly to an average of 6.9. The distribution of the pH_i decreased, with s.d.(pH_{int}) = 0.12, and began showing a single peak. At $t = 10$ min, the pH_i declined to 6.7 and the distribution of the pH_i was very narrow (s.d.(pH_{int}) = 0.06), which was also seen in figure 2. We believe that the reason for this drop in s.d.(pH_{int}) is the merging of cytosolic and vacuolar pH. The pH_i of the cell then dropped from 6.7 to 5.6 over the course of 20 min. The distribution of the pH_i did not change; however, s.d.(pH_{int}) slightly increased again to 0.07. This was most probably caused by the decrease in sensitivity of the probe at low pH values, causing larger variations in the pH_i measurements, as seen in figure 1.

The use of glucose in the buffer gives the cells energy to maintain the activity of the H^+-ATPase [28]; however, our data indicated that it also caused the cells to transport CFDA-SE or CF-SE inside the vacuole, causing a higher concentration of the probe inside the vacuole compared with the cytosol. The requirement of an energy source to transport the probe inside the vacuole was shown by using stained cells placed in the same McIlvaine buffer, but without glucose.

In figure 4, we show the average pH_i development of cells exposed to 30°C, 50°C, 60°C and 70°C. We see that cells suspended in YGP media had an average pH of 7.1 at 30°C. The pH_i of control cells (30°C) decreased from 7.1 to 6.8 in 60 min, indicating that the staining and consequent pH measurements were relatively stable over the measurement period. The drop could be due to relocalization of the probe between the vacuole and the cytosol or a general drop in pH_i of the whole cell. The pH_i regulation of *S. cerevisiae* has been shown to be influenced to some extent by the external pH [6,29].

The cells exposed to 50°C, 60°C and 70°C all showed a significant decrease in the pH_i, and the pH_i declined faster the higher the incubation temperature was. The pH_i of cells incubated at 70°C declined rapidly. At $t = 5$ min, the cells exhibited an exponential decay from where the fit started. The fitted line had an exponential decay rate constant of $k = 0.356$ calculated from equation (2.2). After 15 min, the pH_i of the cells did not drop any further. A slight increase in pH_i between 25 and 30 min occurred, which may be caused by the noise in the measurements owing to the small ratio changes at low pH values with proportionally larger

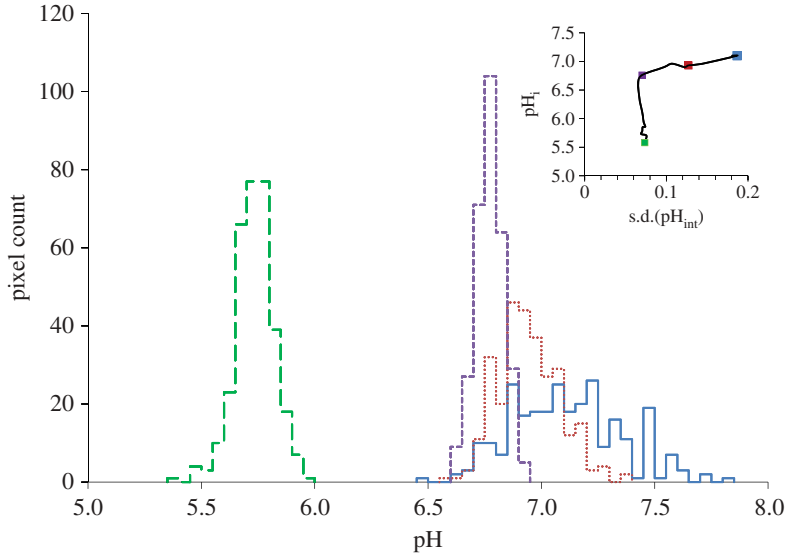

Figure 3. Histogram of the pH_i distribution in a single cell exposed to 60°C at $t = 0$,5,10 and 30 min (blue line, 0 min; red-dotted line, 5 min; magenta short-dashed line, 10 min; green long-dashed line, 30 min). The insert at top right shows the pH_i and the s.d.(pH_{int}) of the same cell. The highlighted data point correspond to the four histograms in the main figure.

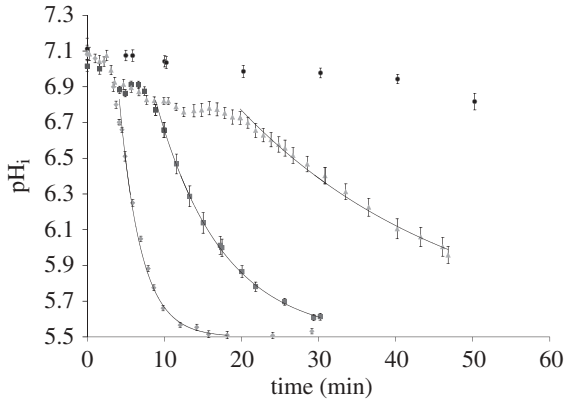

Figure 4. The pH_i of cells incubated at 30°C (filled circles), 50°C (filled triangles), 60°C (filled squares) and 70°C (filled diamonds). Each data point is the average of 30 cells. The error bars are the standard error mean. The fits are single exponential decay functions, the values of which are found in table 1.

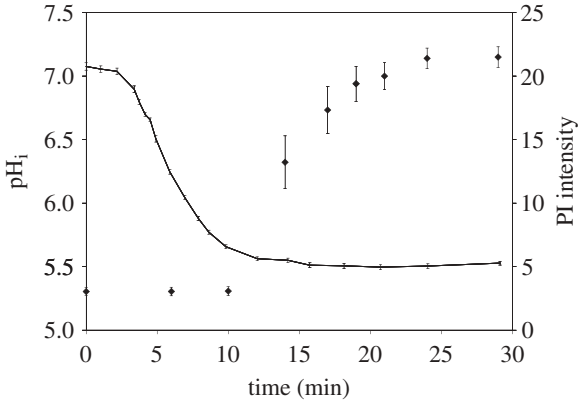

Figure 5. The pH_i (solid line) and the PI (filled diamonds) intensity of cells incubated at 70°C. The pH_i data are taken from figure 4. Each data point is the average of 30 cells. The error bars are the standard error mean. The PI data points represent the average PI intensity of the same 30 cells and the error bars are the standard error mean.

standard deviation compared with the ratio dynamics (figure 1). The pH_i of cells incubated at 60°C decreased slowly until $t = 10$ min. Hereafter, it dropped much faster and almost plateaued at $t = 30$ min at pH 5.6. The exponential fit gave a decay rate constant of $k = 0.117$. The pH_i of cells incubated at 50°C decreased initially at the same rate as the cells incubated at 60°C but continued at the same rate for 20 min. At 20 min, the rate changed and the pH_i dropped more rapidly, reaching a pH_i of 6.5 after 30 min. The fitted exponential decay rate constant was $k = 0.036$.

A criteria for the exponential decay model is that the pH_i distribution is homogeneous, as the model only applies to a simple lipid vesicle with one internal and one external pH. If the pH_i is homogeneous, the associated s.d.(pH_{int}) will be small. From figure 6, it is evident that at the time of the start of the exponential decay, all three s.d.(pH_{int}) values associated with the cells exposed to 50°C, 60°C and 70°C are below 0.07. The pH_i distributions of the cells at the start of the exponential fit are therefore assumed to be homogeneous. In table 1, we have collected values associated with the exponential fit in figure 4, i.e. decay rate constants, goodness of the exponential fit and the calculated plasma membrane proton permeability coefficients from equation (2.3). From table 1, we found a relatively good fit for all three temperatures. We also observed a 10-fold increase in k, and consequently in the calculated permeabilities, from 50°C to 70°C. The start of the exponential decay also decreased significantly as the incubation temperature increased, from 20 min at 50°C to 5 min at 70°C.

In figure 5, the pH_i and the normalized PI intracellular staining intensity of cells incubated at 70°C were plotted. Normalization was done by dividing all PI values with the maximum value at $t = 30$ min. After 10 min, the PI signal was almost zero even though the pH_i was close to pH_{ex}. At $t = 14$ min, the PI signal

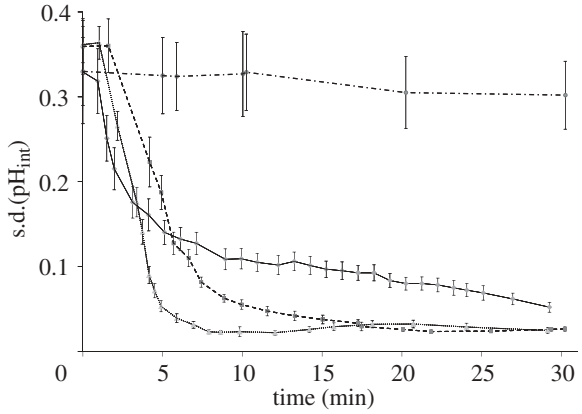

Figure 6. Standard deviation of the intracellular pH of cell incubated at 30°C (filled circles), 50°C (filled diamonds), 60°C (filled squares) and 70°C (filled triangles). Each data point is an average of 30 cells. The error bars are the standard error mean.

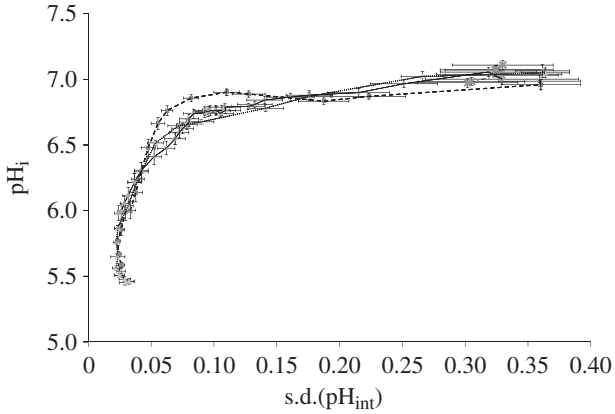

Figure 7. Standard deviation of the intracellular pH versus the pH_i of cells incubated at 30°C (crosses), 50°C (filled diamonds), 60°C (filled squares) and 70°C (filled triangles). Each data point is an average of 30 cells. The error bars are the standard error mean. The data are a combination of figures 4 and 6.

was at half of its maximum value, and after 21 min, it had reached its maximum. The maximum was most probably because of the DNA being saturated by the interaction of the PI probe. This was tested by using half the number of cells and comparing the intensities. The intensities were the same, indicating DNA intercalation saturation (data not shown). Cells incubated at 50°C and 60°C were also stained with PI; however, no PI staining under these conditions was observed (data not shown).

In figure 6, the temporal development of s.d.(pH_{int}) at all four temperatures is shown. We observed that in the first minute there was almost no change in s.d.(pH_{int}). This result was expected, as the temperature, because of the experimental set-up, did not change within that time period [16]. However, after the first 2 min, s.d.(pH_{int}) dropped rapidly, indicating increasing equilibration of the intracellular compartments. The slope of the s.d.(pH_{int}) drop was similar for all three temperatures; however, they decreased their slope at different times. The cells incubated at 70°C changed the rate after 5 min and reached a plateau of 0.03 at $t = 8$ min. The cells incubated at 60°C showed a similar trend but changed the slope at $t = 8$ min and plateaus at $t = 20$ min. The cells exposed to 50°C changed from the initial drop to a more linear drop at 5 min, and at 30 min, the s.d.(pH_{int}) was higher than for the cells exposed to 60°C and 70°C.

In figure 7, we have plotted pH_i versus s.d.(pH_{int}) for the three different temperatures. The graph does not have a time line, but for all three temperatures, the cells started at high pH_i and high s.d.(pH_{int}) and ended at a lower pH_i and a lower s.d.(pH_{int}). All had a similar initial large drop in s.d.(pH_{int}), while the pH_i change was much smaller. At around s.d.(pH_{int}) = 0.07, there was a change for all three temperatures where the pH_i of the cells dropped more rapidly, whereas the s.d.(pH_{int}) change was smaller. For the cells incubated at 50°C, the slope change was very sharp, and the data point at the slope change corresponds to $t = 20$ min, which in figure 4 corresponds to the start of the exponential decay. For the cells incubated at 60°C, the slope change is at $t = 10$ min and also corresponds to the start of the exponential decay in figure 4. The cells incubated at 70°C do not exhibit the same sharp change as the cells exposed to 50°C and 60°C. The change of the slope at pH 6.5–6.7, occurring at $t = 6$–7 min, did not correspond to the start of the exponential decay in figure 4, which occurred at $t = 5$ min.

4. DISCUSSION

It has previously been shown that the yeast vacuole has a pH that is significantly lower than that of the cytosol [30]. From figure 2, we observe similar results, but because of the constraints on our set-up, we were not able to precisely measure cytosolic and vacuolar pH values for all cells. This is also evident in figure 3 where there are no clear peaks representing either the vacuolar or cytosolic pH. Furthermore, the vacuolar pH seen in figure 2 may be overestimated owing to the fact that it is surrounded both above and below by the cytosol. Depending on the relative intensity between the cytosol and the vacuole, the effect will be more or less pronounced. Given the constraints of our set-up, we found it necessary to switch our approach from determining pH values of individual organelles to determining a general pH heterogeneity within the cell. This heterogeneity we define as s.d.(pH_{int}).

As seen in figure 6, the s.d.(pH_{int}) changes as a response to supralethal temperatures. We assume that the changes in s.d.(pH_{int}) are primarily due to changes in cytosolic and vacuolar pH, as they are the largest contributors to the pH_i [30,31]. We believe these pH changes are caused by a combination of permeability changes and thermal deactivation of transporters and pumps in the membranes. It has been shown that the proton permeability of the membrane of intracellular organelles in mammalian cells varies [25]. This is probably caused by differences in membrane composition between the various organelles [32]. Given these facts, the temperature dependence of the permeability is also likely to change. A differential change in permeability could result in the plasma membrane becoming

very permeable to protons as the temperature changes while the vacuolar membrane is less sensitive to temperature changes. This would result in the cytosolic pH dropping towards the vacuolar pH. Furthermore, different temperature-dependent deactivation of membrane H^+-ATPases could result in deactivation of the plasma membrane H^+-ATPases sooner than vacuolar H^+-ATPases, also resulting in a drop in the cytosolic pH. In figure 2, we see indications of this; i.e. the cytosolic pH drops to the same level as the vacuole, which remains stable for 8 min before it drops together with the cytosolic pH. Alternatively, it is possible that the vacuolar membrane permeability is more temperature sensitive than the plasma membrane permeability, or that the plasma membrane H^+-ATPase is more robust to temperature changes than the vacuolar H^+-ATPase. Under these circumstances the consequence of a supralethal temperature increase would be that both cytosolic and vacuolar pH would change, however, the pH_i would remain stable as there is no net flux of protons into the cell but simply a redistribution of the internal pH. We do observe a small drop in the pH_i simultaneously with the s.d.(pH_{int}) drop, indicating the drop in s.d.(pH_{int}) is caused primarily by the lowering of the cytosolic pH. It is of course possible for the two scenarios to happen simultaneously, thereby confounding the effects. To elucidate this would require higher resolution images so as to more accurately determine cytosolic and vacuolar pH.

As intracellular pH gradients are necessary for essential cell functions, a complete dissipation of the intracellular pH gradient will be expected to have detrimental effects on the physiological state of the cell. The results from figure 7 clearly show similar development of the relationship between pH_i and s.d.(pH_{int}) for all three supralethal temperatures, indicating that the thermal stress mechanisms affecting the cells do not vary significantly as a function of temperature between 50°C and 70°C.

The results from figures 6 and 7 also clearly demonstrate that an exponential drop in pH_i will be preceded by a drop in s.d.(pH_{int}). On the basis of the above-mentioned findings, we strongly believe that s.d.(pH_{int}) could be used as an early indicator of the physiological state of *S. cerevisiae* cells exposed to heat stress. Furthermore, in cases where pH_i and pH_{ex} are very close, pH_i measurements to assess cell health/vitality will be meaningless as no change in pH_i will occur. However, measurements of s.d.(pH_{int}) will still be possible to perform.

It should be noted that cytosolic and vacuolar pH values of unstressed cells may vary in different yeast species, and perhaps even in different strains within a species. This could strongly influence the sensitivity of the s.d.(pH_{int}) metric and thereby its usefulness as an early health indicator of other yeast strains than the one used in this study. Further investigation is, however, required to elucidate this hypothesis.

The cells exposed to 50°C, 60°C and 70°C experience an initial phase where the pH_i decreases, slightly suggesting that the cells are still actively trying to control the pH_i. As seen in figure 4, the time of the start of the exponential decay changes inversely with temperature. This indicates that the deactivation of the transporters and pumps is dependent on both time and temperature. After the initial phase, an exponential decay phase then follows, where the pH_i of the cells decreases towards pH_{ex} (figure 4). The relatively good single exponential fit suggests that only passive diffusion controls the change in pH_i after the start of the exponential decay [23,33]. As thermal deactivation of transporters and pumps in the cell membrane occurs, the cell will lose the ability to actively regulate the pH_i. The decay rate constants of the three temperatures are therefore thought to reflect the diffusion of protons through the membrane and not any active transport mechanism. To the best of our knowledge, the results in table 1 are the first of their kind showing heat stress effects on *in vivo* plasma membrane proton permeability coefficients in yeast. Our results demonstrate that plasma membrane proton permeability coefficients in yeast increase with a factor of 10 *in vivo*, as the temperature is increased by 20°C. Plasma membranes isolated from *Bacillus substilis* showed a factor 10 increase in the membrane permeability to protons when the temperature changed to 30°C [34], which agrees well with our data.

The temperature dependence of the pH_i drop is to some extent in agreement with other findings [14]. Using ^{31}P NMR, a drop of 0.7 in pH_i within 5 min of a wild-type *S. cerevisiae* strain 3236 exposed to 52°C has been observed [14]. This is in contrast to our findings, which show a much smaller decrease in pH_i within 5 min. However, these authors used a lower pH_{ex}, which would result in a larger pH_i drop. In addition, they kept the cells on ice before subjecting them to lethal temperatures, thereby increasing the relative temperature difference to which the cells were subjected. This could make the cells more temperature sensitive compared with our cells. Temperature dependence on deactivation of plasma membrane H^+-ATPase is also very dependent on species [13,35]. It is therefore plausible that large variations in pH_i regulation between strains of *S. cerevisiae* may exist. Furthermore, the membrane permeability has been shown to be dependent on the pH_{ex} [24], further complicating direct comparisons of pH_i value drops between different experiments.

In figure 5, a significant lag between the start of pH_i decrease in cells and the beginning of PI staining of DNA at 70°C is evident. This shows that cell membrane integrity is maintained for an extended period even though the pH_i of the cell is decreasing. This is in contrast to other findings, which using ethidium bromide to detect membrane integrity, observed increased fluorescence from ethidium bromide after 3 min [14]. Membrane permeability for ethidium bromide may be higher than for PI, which would explain the differences. Whether the rupture of the plasma membrane is dependent on the incubation time is unclear from our findings and further studies are needed to elucidate this.

In conclusion, this study reports for the first time on the use of FRIM to measure *in vivo* plasma membrane proton permeability coefficients in yeast. Furthermore, we have demonstrated that the start of the exponential pH_i decay and the rupture of the cell plasma membrane at 70°C are not simultaneous but are separated by a

significant temporal difference, further stressing the fact that PI staining alone does not portray an accurate account of cellular viability. Finally, we have introduced a new metric s.d.(pH_{int}) and shown its possible use as an early health/vitality indicator in *S. cerevisiae* cells during heat stress.

REFERENCES

1 Patel, P. & Markx, G. 2008 Dielectric measurement of cell death. *Enzyme Microb. Technol.* **43**, 463–470. (doi:10.1016/j.enzmictec.2008.09.005)

2 Bright, G., Fisher, G. & Rogowska, J. D. L. 1987 Fluorescence ratio imaging microscopy: temporal and spatial measurements of cytoplasmic pH. *J. Cell Biol.* **104**, 1019–1033. (doi:10.1083/jcb.104.4.1019)

3 Diwu, Z., Chen, C., Zhang, C., Klaubert, D. & Haugland, R. 1999 A novel aciclotropic pH indicator and its potential in labeling acidic organelles of live cells. *Chem. Biol.* **6**, 411–418. (doi:10.1016/S1074-5521(99)80059-3)

4 Smigic, N., Rajkovic, A., Nielsen, D. S., Arneborg, N., Siegumfeldt, H. & Devlieghere, F. 2010 Survival of lactic acid and chlorine dioxide treated *Campylobacter jejuni* under suboptimal conditions of pH, temperature and modified atmosphere. *Int. J. Food Microbiol.* **141**, 140–146. (doi:10.1016/j.ijfoodmicro.2010.01.026)

5 Tholozan, J. L. *et al.* 1999 Physiological characterization of viable-but-nonculturable *Campylobacter jejuni* cells. *Appl. Environ. Microbiol.* **65**, 1110–1116.

6 Imai, T. & Ohno, T. 1995 The relationship between viability and intracellular pH in the yeast *Saccharomyces cerevisiae*. *Appl. Environ. Microbiol.* **61**, 3604–3608.

7 Mortensen, H. D., Gori, K., Siegumfeldt, H., Nissen, P., Jespersen, L. & Arneborg, N. 2006 Intracellular pH homeostasis plays a role in the NaCl tolerance of *Debaryomyces hansenii* strains. *Appl. Microbiol. Biotechnol.* **71**, 713–719. (doi:10.1007/s00253-005-0196-2)

8 Serrano, R., Kielland-Brandt, M. & Fink, G. 1986 Yeast plasma membrane ATPase is essential for growth and has homology with (Na^++K^+), K^+-and Ca^{2+}-ATPases. *Nature* **319**, 689–693. (doi:10.1038/319689a0)

9 Spilimbergo, S., Bertucco, A., Basso, G. & Bertoloni, G. 2005 Determination of extracellular and intracellular pH of *Bacillus subtilis* suspension under CO_2 treatment. *Biotechnol. Bioeng.* **92**, 447–451. (doi:10.1002/bit.20606)

10 Valli, M., Sauer, M., Branduardi, P., Borth, N., Porro, D. & Mattanovich, D. 2006 Improvement of lactic acid production in *Saccharomyces cerevisiae* by cell sorting for high intracellular pH. *Appl. Environ. Microbiol.* **72**, 5492–5499. (doi:10.1128/AEM.00683-06)

11 Han, J. & Burgess, K. 2010 Fluorescent indicators for intracellular pH. *Chem. Rev.* **110**, 2709–2728. (doi:10.1021/cr900249z)

12 Piper, P. W. 1993 Molecular events associated with acquisition of heat tolerance by the yeast *Saccharomyces cerevisiae*. *FEMS Microbiol. Rev.* **11**, 339–355. (doi:10.1111/j.1574-6976.1993.tb00005.x)

13 Sampedro, J. G., Cortés, P., Muñoz-Clares, R. A., Fernández, A. & Uribe, S. 2001 Thermal inactivation of the plasma membrane H^+-ATPase from *Kluyveromyces lactis*. Protection by trehalose. *Biochim. Biophys. Acta* **1544**, 64–73. (doi:10.1016/S0167-4838(00)00205-3)

14 Coote, P. J., Jones, M. V., Seymour, I. J., Rowe, D. L., Ferdinando, D. P., McArthur, A. J. & Cole, M. B. 1994 Activity of the plasma membrane H^+-ATPase is a key physiological determinant of thermotolerance in *Saccharomyces cerevisiae*. *Microbiology* (*Reading, England*) **140**, 1881–1890. (doi:10.1099/13500872-140-8-1881)

15 McIlvaine, T. C. 1921 A buffer solution for colorimetric comparison. *J. Biol. Chem.* **49**, 183–186.

16 Aabo, T. *et al.* Submitted. BWS: a versatile setup for simultaneous optical manipulation, heat stress and intracellular pH measurements of live cells. *Rev. Sci. Instrum.*

17 Bright, G. *et al.* 1989 *Methods in cell biology: fluorescence ratio imaging microscopy*. New York, NY: Academic Press.

18 Kastbjerg, V. G., Nielsen, D. S., Arneborg, N. & Gram, L. 2009 Response of *Listeria monocytogenes* to disinfection stress at the single-cell and population levels as monitored by intracellular pH measurements and viable-cell counts. *Appl. Environ. Microbiol.* **75**, 4550–4556. (doi:10.1128/AEM.02625-08)

19 Rasmussen, M. B., Oddershede, L. B. & Siegumfeldt, H. 2008 Optical tweezers cause physiological damage to *Escherichia coli* and *Listeria* bacteria. *Appl. Environ. Microbiol.* **74**, 2441–2446. (doi:10.1128/AEM.02265-07)

20 Sezgin, M. & Sankur, B. 2004 Survey over image thresholding techniques and quantitative performance evaluation. *J. Electron. Imaging* **13**, 146–165. (doi:10.1117/1.1631315)

21 Grabe, M. & Oster, G. 2001 Regulation of organelle acidity. *J. Gen. Physiol.* **117**, 329–344. (doi:10.1085/jgp.117.4.329)

22 Rybak, S. 1997 Theoretical considerations on the role of membrane potential in the regulation of endosomal pH. *Biophys. J.* **73**, 674–687. (doi:10.1016/S0006-3495(97)78102-5)

23 Elamrani, K. & Blume, A. 1983 Effect of the lipid phase transition on the kinetics of H^+/OH^--diffusion across phosphatidic acid bilayers. *Biochim. Biophys. Acta* **727**, 22–30. (doi:10.1016/0005-2736(83)90364-4)

24 Miedema, H., Staal, M. & Prins, H. 1996 pH-induced proton permeability changes of plasma membrane vesicles. *J. Membr. Biol.* **152**, 159–167. (doi:10.1007/s002329900094)

25 Wu, M. M., Grabe, M., Adams, S., Tsien, R. Y., Moore, H.-P. H. & Machen, T. E. 2001 Mechanisms of pH regulation in the regulated secretory pathway. *J. Biol. Chem.* **276**, 33 027–33 035. (doi:10.1074/jbc.M103917200)

26 Zeng, J., Smith, K. & Chong, P. 1993 Effects of alcohol-induced lipid interdigitation on proton permeability in L-alpha-dipalmitoylphosphatidylcholine vesicles. *Biophys. J.* **65**, 1404–1414. (doi:10.1016/S0006-3495(93)81204-9)

27 Roos, W., Evers, S., Hieke, M., Tschöpe, M. & Schumann, B. 1998 Shifts of intracellular pH distribution as a part of the signal mechanism leading to the elicitation of benzophenanthridine alkaloids. Phytoalexin biosynthesis in cultured cells of *Eschscholtzia californica*. *Plant Physiol.* **118**, 349–364. (doi:10.1104/pp.118.2.349)

28 Ramos, S. *et al.* 1989 The mechanism of intracellular acidification induced by glucose in *Saccharomyces cerevisiae*. *J. Gen. Microbiol.* **135**, 2413–2422.

29 Valmorri, S., Mortensen, H., Jespersen, L., Corsetti, A., Gardini, F., Suzzi, G. & Arneborg, N. 2008 Variations of internal pH in typical Italian sourdough yeasts during co-fermentation with lactobacilli. *LWT Food Sci. Technol.* **41**, 1610–1615. (doi:10.1016/j.lwt.2007.11.006)

30 Vindeløv, J. & Arneborg, N. 2002 *Saccharomyces cerevisiae* and *Zygosaccharomyces mellis* exhibit different hyperosmotic shock responses. *Yeast* **19**, 429–439. (doi:10.1002/yea.844)

31 Orij, R., Postmus, J., Ter Beek, A., Brul, S. & Smits, G. J. 2009 *In vivo* measurement of cytosolic and mitochondrial pH using a pH-sensitive GFP derivative in *Saccharomyces*

cerevisiae reveals a relation between intracellular pH and growth. *Microbiology* **155**, 268–278. (doi:10.1099/mic.0.022038-0)

32 Zinser, E. & Daum, G. 1995 Isolation and biochemical characterization of organelles from the yeast, *Saccharomyces cerevisiae*. *Yeast* (*Chichester, England*) **11**, 493–536. (doi:10.1002/yea.320110602)

33 Redelmeier, T. E., Mayer, L. D., Wong, K. F., Bally, M. B. & Cullis, P. R. 1989 Proton flux in large unilamellar vesicles in response to membrane potentials and pH gradients. *Biophys. J.* **56**, 385–393. (doi:10.1016/S0006-3495(89)82684-0)

34 Van De Vossenberg, J. L. *et al.* 1999 Homeostasis of the membrane proton permeability in *Bacillus subtilis* grown at different temperatures. *Biochim. Biophys. Acta* **1419**, 97–104. (doi:10.1016/S0005-2736(99)00063-2)

35 Felix, C. F., Moreira, C. C., Oliveira, M. S., Sola-Penna, M., Meyer-Fernandes, J. R., Scofano, H. M. & Ferreira-Pereira, A. 1999 Protection against thermal denaturation by trehalose on the plasma membrane H^+-ATPase from yeast. Synergetic effect between trehalose and phospholipid environment. *Eur. J. Biochem.* **266**, 660–664. (doi:10.1046/j.1432-1327.1999.00916.x)